Optical and near-infrared integral field spectroscopy of the SCUBA galaxy N2 850.4

William C. Keel – University of Alabama
et al.

Citation of published version:

Swinbank, A. et al. (2005): Optical and near-infrared integral field spectroscopy of the SCUBA galaxy N2 850.4. *Monthly Notices of the Royal Astronomical Society*, 359(2). DOI: https://doi.org/10.1111/j.1365-2966.2005.08901.x

Mon. Not. R. Astron. Soc. **359,** 401–407 (2005) doi:10.1111/j.1365-2966.2005.08901.x

Optical and near-infrared integral field spectroscopy of the SCUBA galaxy N2 850.4

A. M. Swinbank,[1⋆] Ian Smail,[1] R. G. Bower,[1] C. Borys,[2] S. C. Chapman,[2] A. W. Blain,[2] R. J. Ivison,[3,4] S. Ramsay Howat,[3] W. C. Keel[5] and A. J. Bunker[6]

[1]*Institute for Computational Cosmology, Department of Physics, University of Durham, South Road, Durham DH1 3LE*
[2]*Astronomy Department, California Institute of Technology, 105-24, Pasadena, CA 91125, USA*
[3]*Astronomy Technology Centre, Royal Observatory, Blackford Hill, Edinburgh EH9 3HJ*
[4]*Institute for Astronomy, University of Edinburgh, Royal Observatory, Blackford Hill, Edinburgh EH9 3HJ*
[5]*Department of Physics and Astronomy, University of Alabama, Tuscaloosa, AL 35487, USA*
[6]*Department of Physics, University of Exeter, Stocker Road, Exeter EX4 4QL*

Accepted 2005 February 3. Received 2005 February 3; in original form 2004 December 6

ABSTRACT

We present optical and near-infrared integral field spectroscopy of the SCUBA galaxy SMM J163650.43+405734.5 (ELAIS N2 850.4) at $z = 2.385$. We combine Lyα and Hα emission line maps and velocity structure with high-resolution *HST* ACS and NICMOS imaging to probe the complex dynamics of this vigorous starburst galaxy. The imaging data show a complex morphology, consisting of at least three components separated by $\sim$1 arcsec (8 kpc) in projection. When combined with the Hα velocity field from UKIRT UIST IFU observations we identify two components whose redshifts are coincident with the systemic redshift, measured from previous CO observations, one of which shows signs of AGN activity. A third component is offset by 220 ± 50 km s^{-1} from the systemic velocity. The total star-formation rate of the whole system (estimated from the narrow-line Hα and uncorrected for reddening) is 340 ± 50 M$_\odot$ yr^{-1}. The Lyα emission mapped by the GMOS IFU covers the complete galaxy and is offset by $+270 \pm 40$ km s^{-1} from the systemic velocity. This velocity offset is comparable to that seen in rest-frame UV-selected galaxies at similar redshifts and usually interpreted as a starburst-driven wind. The extended structure of the Lyα emission suggests that this wind is not a nuclear phenomenon, but is instead a galactic-scale outflow. Our observations suggest that the vigorous activity in N2 850.4 is arising as a result of an interaction between at least two dynamically-distinct components, resulting in a strong starburst, a starburst-driven wind and actively-fuelled AGN activity. Whilst these observations are based on a single object, our results clearly show the power of combining optical and near-infrared integral field spectroscopy to probe the power sources, masses and metallicities of far-infrared luminous galaxies, as well as understanding the role of AGN- and starburst-driven feedback processes in these high-redshift systems.

Key words: stars: formation – galaxies: active – galaxies: evolution – galaxies: high-redshift – galaxies: individual: SMM J163650.43+405734.5 (N2 850.4).

1 INTRODUCTION

Recent surveys have concluded that a substantial fraction of the high-redshift submillimetre (sub-mm) selected galaxy population comprises morphologically complex systems with high instantaneous star-formation rates and actively fuelled AGNs (Smail, Ivison & Blain 1997; Barger et al. 1999; Ivison et al. 2002; Scott et al. 2002; Smail et al. 2002; Alexander et al. 2003, 2005; Chapman et al. 2003; Webb et al. 2003; Dannebauer et al. 2004; Knudsen 2004; Swinbank et al. 2004; Chapman et al. 2005; Pope et al. 2005). Understanding the importance of this population requires identifying their power source (e.g. to determine whether star formation or AGN activity dominate the luminosity output) and, perhaps more importantly, masses for these galaxies. Although they have only moderate space densities, their apparently high star-formation rates mean their contribution to the cosmic star-formation rate could be significant (e.g. Chapman et al. 2004). Moreover, the

⋆E-mail: a.m.swinbank@durham.ac.uk

star-formation activity suggests a priori that these galaxies should house starburst-driven superwinds – outflows that expel gas from the galaxy potential (e.g. Pettini et al. 2001; Shapley et al. 2003) and that are believed to play an important role in regulating galaxy formation, preventing the bulk of baryons cooling into stars (the 'cosmic cooling crisis', White & Rees 1978; Cen & Ostriker 1999; Balogh et al. 2001). However, to study the energetics and dynamics of these frequently complex systems (e.g. Smail et al. 2004) we must trace the distribution of the velocity and intensity of emission lines on sub-arcsecond scales. Ideally, this should be achieved in 2-D to untangle the complex morphologies of these systems and, in addition, to search for signatures of lensing, which might provide a more mundane explanation of the apparently intense luminosities of these galaxies (Tecza et al. 2004).

In this paper we demonstrate the power of combining optical and near-infrared integral field spectroscopy with high-resolution *Hubble Space Telescope* (*HST*) imaging to study the dynamics, morphologies, masses and outflows of SCUBA galaxies. Using the Integral Field Units (IFUs) on GMOS (optical) and UIST (near-infrared) we have studied the SCUBA galaxy SMM J163650.43+405734.5 (ELAIS N2 850.4) (Ivison et al. 2002; Scott et al. 2002; Smail et al. 2003). In Section 2 we present the data reduction and results from the spectroscopic and imaging data. In Sections 3 and 4 we present our analysis and conclusions, respectively. We use a cosmology with $H_0 = 70$ km s^{-1}, $\Omega_M = 0.3$ and $\Omega_\Lambda = 0.7$ in which 1 arcsec corresponds to 8.2 kpc at $z = 2.4$.

2 OBSERVATIONS AND ANALYSIS

N2 850.4 was first catalogued as a bright (8.2 ± 1.7 mJy) sub-mm source by Scott et al. (2002) and identified through its radio counterpart by Ivison et al. (2002). A spectroscopic redshift of $z = 2.38$ for the radio counterpart was measured by Chapman et al. (2003, 2005). N2 850.4 has a far-infrared bolometric luminosity of $L_{FIR} = 3.1 \times 10^{13}\ L_\odot$ (Chapman et al. 2005), which corresponds to a star-formation rate of $\sim$5400 $M_\odot$ yr^{-1} (Kennicutt 1998), although the far-infrared luminosity may have a contribution from a non-thermal (AGN) component. Interferometric observations of the molecular CO emission in this system by Neri et al. (2003) have tied down the systemic redshift as $z = 2.384 \pm 0.001$ and indicate a gas mass of $5.5 \times 10^{10}\ M_\odot$. The system was studied in detail by Smail et al. (2003), whose multi-wavelength long-slit observations suggest that this system comprises at least two components, one of which has a Seyfert-like AGN and the other maybe a UV-bright starburst with an outflow. These observations show extended [O III] λ5007 emission as well as strong UV stellar absorption features.

However, owing to the multi-component nature of this system and the way in which long-slit observations mix spatial and spectral resolution, observations of this galaxy have been difficult to interpret (Smail et al. 2003). By targeting N2 850.4 with an IFU we are able to decouple the spatial and spectral resolution and cleanly probe the dynamics and power sources of this hyper-luminous SCUBA galaxy.

2.1 *HST* optical and near-infrared imaging

HST Advanced Camera for Surveys (ACS) observations were obtained from the *HST* public archive[1] (Programme ID #9761). The data consist of dithered exposures with the F814W filter, taken in LOWSKY conditions using the default four-point ACS-WFC-DITHER-BOX configuration. This pattern ensures optimal half-pixel sampling along both coordinates. The total integration time was 4.8 ks. We reduced the data using the latest version of the MULTIDRIZZLE software (Koekemoer et al. 2002) using the default parameters with PIXFRAC $= 1$ and SCALE $= 1$. The resulting image has 0.05-arcsec pixels and is free from artifacts (Fig. 1).

The NICMOS data were obtained in Cycle 12, and the target was observed using the NIC2 camera in the F160W filter for a total of 2.3 ks (Program ID #9856). We employed the standard four-point spiral dither pattern, LOWSKY conditions and used the MULTIACCUM readmode. Each exposure was corrected for a pedastal offset, and then mosaiced using the CALNICB task in IRAF. Unfortunately, the observation was affected by the South Atlantic Anomaly (SAA), and extra processing steps were required.[2] The final images appear very flat and have very low cosmic ray contamination. Absolute astrometry of the NICMOS images is accurate to only $\leqslant$2 arcsec, so we cross-correlated the full image against the high-resolution ACS data to align the near-infrared image with the optical image. Both are aligned with the FK5 coordinate system of our deep radio map of this field (Ivison et al. 2002) which has an absolute astrometry precision of 0.3 arcsec. A complete discussion of the optical and near-infrared observations and data-reduction is given in Borys et al. (in preparation).

We degrade the *HST* ACS data to the same resolution as the NICMOS observations and make a true colour ($I_{814}H_{160}$) image of N2 850.4. An inspection of this imaging data (Fig. 1) reveals a complex system made up of several components. In particular, the brightest features have similar colours and an apparent geometry which is reminiscent of a triply-imaged, strongly lensed system. Could the immense luminosity of N2 850.4 be due to strong lensing (e.g. Chapman et al. 2002)? Our IFU observations of this system provide a powerful tool for testing this suggestion, since the redshifts and spectral features should be the same for all three components if they are all images of a single background galaxy.

2.2 IRTF narrow-band imaging

Narrow-band imaging of N2 850.4 was carried out using the 3-m NASA Infra-Red Telescope Facility (IRTF) Telescope between 2003 April 28 and 2003 May 02. The observations were made in generally photometric conditions and $\sim$0.7-arcsec seeing. We used the NSFCAM camera (Shure et al. 1993) which employs a 256×256 InSb detector at 0.15 arcsec pixel^{-1} to give a 38-arcsec field of view (which probes roughly 300 kpc at $z \sim 2.4$). The continuously variable tunable narrow-band filter (CVF) in NSFCAM provides an $R = 90$ passband which was tuned to target the Hα emission at the systemic galaxy redshift measured ($z = 2.384$) from the CO and UV spectra of Neri et al. (2003) and Smail et al. (2003), respectively. Shorter, matched broad-band imaging was interspersed between the narrow-band exposures to provide continuum subtraction. The total narrow-band integration time was 19.8 ks and the total broad-band integration time was 2.2 ks. These observations, their reduction and analysis are discussed in detail in Swinbank et al. (2004).

[1] Obtained from the Multimission Archive at the Space Telescope Science Institute (MAST).

[2] For a full description, see http://www.stsci.edu/hst/nicmos/tools/post_SAA_tools.html.

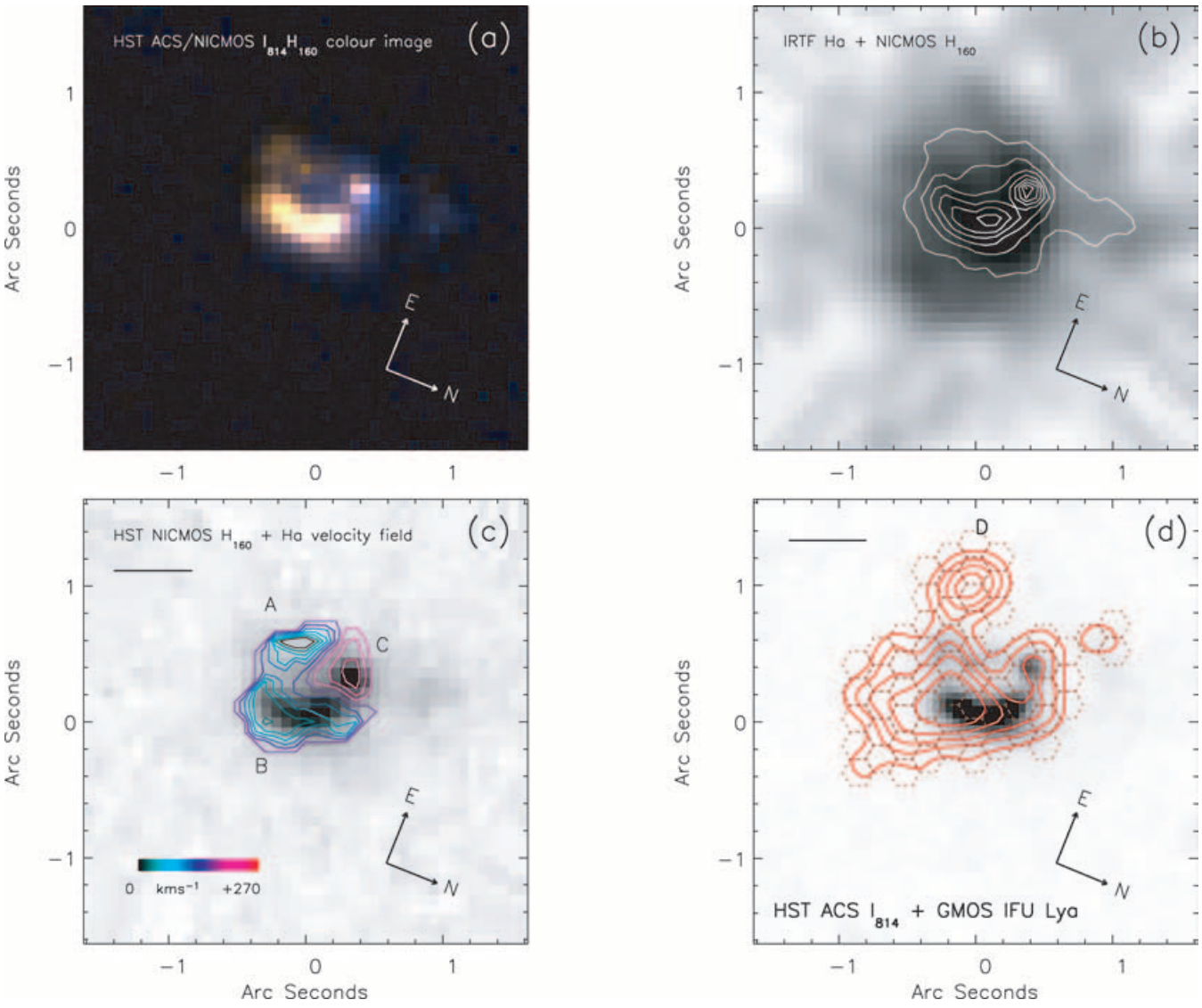

Figure 1. (a) True colour I_{814} H_{160} image of N2 850.4 from the *HST* ACS and NICMOS imaging. The image shows a complex morphology, with at least three distinct components separated by ∼1 arcsec (∼8 kpc) in projection. (b) IRTF Hα narrow-band image of N2 850.4 with the contours from the NICMOS H_{160}-band image overlaid. This Hα narrow-band image shows a diffuse halo of material distributed asymmetrically around the galaxy (seeing ∼0.7 arcsec). (c) The velocity field of N2 850.4 derived from UIST IFU observations of the Hα emission line overlaid on the NICMOS H_{160}-band image. The redshift of component *A* is in excellent agreement with previous CO observations (Neri et al. 2003). Components *A* and *B* are separated by 50 ± 50 km s^{-1} whilst there is a velocity difference of $+270 \pm 50$ km s^{-1} between components *A* and *C* (the 0.6 arcsec seeing is marked by the solid bar in the top left-hand corner). (d) *HST* ACS I_{814}-band (F814) image of N2 850.4 with the Lyα intensity from the GMOS IFU overlaid as contours (the contours mark 3, 4, 5, 6 and 7σ). We also overlay the footprint of the GMOS IFU fibres that have >3σ emission line detections. The solid bar in the top left-hand corner of this panel represent 0.6 arcsec seeing. The Lyα contours match the high surface brightness emission traced by the I_{814}-band imaging data, although there is Lyα emission to the East (labelled *D*) that is not seen in the I_{814}-band morphology. The Lyα is redshifted from the systemic by $+270 \pm 40$ km s^{-1}, which may be indicative of a galactic-scale outflow.

2.3 Spectroscopic imaging

2.3.1 UIST near-infrared integral field spectroscopy

Observations of N2 850.4 were made in queue mode with the UKIRT Image-Spectrometer (UIST) IFU between 2003 March 27 and 2003 April 04 in <0.6-arcsec seeing and photometric conditions. The UIST IFU uses an image slicer and re-imaging mirrors to reformat a square array of 14 slices of the sky (each 0.24 arcsec×0.12 arcsec) into a pseudo long slit. The resulting field of view is 3.4 arcsec × 6.0 arcsec (Ramsay et al. 2004). We used the *HK* grism which has a spectral resolution of $\lambda/\Delta\lambda = 1000$ and covers a wavelength range of 1.4–2.4 μm. Observations were carried out in the standard ABBA configuration in which we chopped away to sky by 12 arcsec to achieve good sky subtraction. Individual exposures were 240 s and each observing block was 7.2 ks, which was repeated four times, thus the total integration time was 28.8 ks.

To reduce the data we used the relevant ORAC-DR pipeline (Cavanagh et al. 2003) which sky-subtracts, extracts, wavelength calibrates, flatfields and forms the datacube. In order accurately to align and mosaic the four datacubes, we created white-light (wavelength-collapsed) images around the redshifted Hα emission line from each observing block and used the peak intensity to

centroid the object in the IFU datacube. We then spatially aligned and co-added the four individual datacubes (weighted by Hα S/N) using MOSAIC in KAPPA.

To search for velocity structure we attempted to identify Hα emission on a pixel-by-pixel basis by averaging over a 0.48 arcsec$\times$0.48 arcsec region (4 $\times$ 2 pixels), increasing to 0.6 arcsec$\times$0.72 arcsec (5 $\times$ 3 pixels) if no emission line could initially be identified. At $z = 2.385$, Hα λ6562.8 emission falls at 2.221 μm, which is away from any strong OH emission or absorption. We attempted not only to fit a single Gaussian to the Hα emission line, but also to identify an [N II] λ6583 emission line, only accepting the fit if the χ^2 was significantly better than without the [N II] line. We checked the wavelength calibration of each IFU pixel by fitting a nearby sky line with a Gaussian profile. The errors in the velocity field are calculated by building two independent datacubes, each of 14.4 ks, and recomputing the velocity field in a manner identical with that described above. Using the same fitting techniques as above we estimate the average velocity error to be $\simeq$50 km s^{-1}. Spectra from the three components identified in the UIST IFU observations are shown in Fig. 2.

To confirm the velocity gradients seen in the UIST IFU data (Fig. 1) we also obtained a 4.8-ks exposure around the Hα emission lines with the Keck near-infrared long-slit spectrograph. We aligned the slit along components *A* and *B* in Fig. 1 and derived the same velocity offsets between components as in our IFU data (the spectra and line fluxes are shown and discussed in Swinbank et al. 2004).

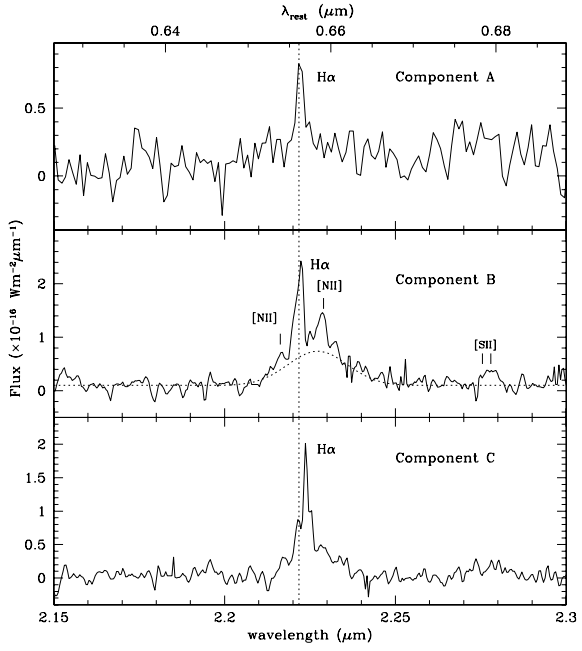

Figure 2. Top: near-infrared spectrum of component *A* around the Hα emission line. This component is at the same redshift as the systemic redshift ($z = 2.384$) as measured from the molecular CO emission by Neri et al. (2003). Middle: near-infrared spectrum of component *B* from which shows a $+50 \pm 50$ km s^{-1} velocity shift from the systemic. This component also has a broad Hα regions offset by $+800 \pm 150$ km s^{-1} which indicates AGN activity. The FWHM of the broad line is 2300 ± 250 km s^{-1}. Lower: near-infrared spectrum of component *C* which shows a 220 ± 50 km s^{-1} velocity offset from the systemic. Component *C* also displays a broad-line component (FWHM $= 1800 \pm 300$ km s^{-1}) which is at a similar redshift to the broad line seen in component *B* and may arise due to the same scattering seen in [O III] λ5007 seen by Smail et al. (2003). The top panel has been binned by a factor of two in the spectral direction to enhance the contrast of the Hα emission. The dotted line shows the wavelength for Hα expected at the systemic redshift of 2.384 (Neri et al. 2003; Smail et al. 2003).

2.3.2 *GMOS optical integral field spectroscopy*

N2 850.4 was observed with the GMOS-IFU on Gemini North on 2002 June 12 during Science Demonstration time for a total of 7.2 ks in 0.6-arcsec seeing and photometric conditions.[3] The GMOS IFU uses a lensed fibre system to reformat a 7 arcsec$\times$ 5 arcsec field into two long slits (Allington-Smith et al. 2002). Using a *B*-band filter in conjunction with the B600 grating results in two tiers of spectra recording the maximum field of view. The spectral resolution of this configuration is $\lambda/\Delta\lambda_{\rm FWHM} = 2000$. For the galaxy at $z = 2.385$, the Lyα emission falls at λ4112 which is in a region of not only low sky emission, but also of low throughput.

The GMOS data reduction pipeline was modified such that the extracted spectra included the blue edge of the CCD (where the Lyα emission falls) and then used to extract and wavelength calibrate the spectra of each IFU element. The variations in fibre-to-fibre response were removed using the continuum around the expected range of Lyα emission. To check the wavelength calibration around λ4100, we wavelength calibrated the CuAr arc observations and fitted the arc lines between $\lambda\lambda$4000 and 4200 with Gaussian profiles. We measured the rms offset between the observed arc line centroids and the arc line list to be less than λ0.02 (which corresponds to less than 8 km s^{-1} in the rest frame of the galaxy). This gives us confidence that any velocity structures or offsets in the GMOS IFU data are real and not simply an artifact of the observations. To search for velocity structure, the spectra were averaged over a 3 $\times$ 3 pixel (0.6 arcsec$\times$0.6 arcsec) spatial region, except where the signal was too low to give a significant detection of the line, in which case the smoothing area was increased to 4 $\times$ 4 pixels. In regions where this averaging process still failed to give an adequate χ^2 (i.e. the inclusion of an emission line component did not improve the fit), no fit was made. In order to detect and fit the line we required a minimum S/N of three and checked every fit by eye. In the inner regions of the galaxy all of the Gaussian profile fits are accepted, while in the outer regions we reject fits if the line centroid was greater than 3000 km s^{-1} away from the systemic, or the best-fit Gaussian profile had a width greater than FWHM $>$3000 km s^{-1}. Although the Lyα emission was resolved (FWHM$\sim$700 km s^{-1}), we detected no significant coherent velocity gradient across the system and placed a limit of 100 km s^{-1} on possible velocity structure (Table 1). We constructed a *Lyα intensity map* from the emission line and overlaid this on the *HST* ACS image in Fig. 1.

3 ANALYSIS

In order to obtain spatially aligned imaging and spectroscopy observations, we began by constructing an Hα image from the UIST IFU and aligned this with the IRFT Hα and continuum images (which were also aligned with the NICMOS and ACS images using stars in the field of view). Furthemore, to tie these to the GMOS data, we

[3] Programme ID: GN-2002A-DD-4. Obtained at the Gemini Observatory, which is operated by the Association of Universities for Research in Astronomy, Inc., under a cooperative agreement with the NSF on behalf of the Gemini partnership: the National Science Foundation (United States), the Particle Physics and Astronomy Research Council (United Kingdom), the National Research Council (Canada), CONICYT (Chile), the Australian Research Council (Australia), CNPq (Brazil) and CONICET (Argentina).

Table 1. Velocities of rest frame UV and optical emission.

Component	$z_{\mathrm{H}\alpha}$	FWHM$_{\mathrm{H}\alpha}$ (km s^{-1})	Hα Flux (10^{-19} W m^{-2})	$z_{\mathrm{Ly}\alpha}$	$v_{\mathrm{H}\alpha}$ (km s^{-1})	$v_{\mathrm{Ly}\alpha}$ (km s^{-1})
A	2.3841[4]	330 ± 40	0.9 ± 0.2	–	0 ± 50	–
B	2.3847[3]	360 ± 25	4.4 ± 0.9	2.3870[4]	$+50 \pm 50$	$+260 \pm 40$
B_{broad}	2.3930[10]	2300 ± 250	16.7 ± 2.0	–	$+800 \pm 150$	–
C	2.3866[3]	320 ± 30	4.0 ± 1.0	2.3872[4]	$+220 \pm 50$	$+275 \pm 40$
C_{broad}	2.3900[12]	1800 ± 300	8.0 ± 1.5	–	$+550 \pm 200$	–
D	–	–	–	2.3860[6]	–	$+170 \pm 50$

Notes: the values given in square brackets in the z-columns are the errors in the last decimal place. The quoted velocities are with respect to the systemic redshift from Neri et al. (2003).

constructed an Lyα and continuum image from the GMOS IFU and aligned these with the galaxy in an observed V-band image from Ivison et al. (2002). This V-band image was then aligned with the near-infrared imaging, resulting in accurate alignment between the GMOS, UIST, IRTF and HST observations. We estimate the uncertainty in the astrometry between any two frames to be $\lesssim$0.2 arcsec. Having combined the *HST* H_{160} and I_{814}-band NICMOS and ACS imaging with the velocity structure of the Hα emission, we found at least three dynamically distinct components (labelled *A*, *B* and *C* in Fig. 1) and the near-infrared spectra around the Hα emission from these components are shown in Fig. 2. The redshift of components *A* and *B* are in excellent agreement with previous CO(4–3) observations, which measured the systemic redshift to be 2.384 ± 0.001 (Neri et al. 2003; Greve et al. 2005). The other component, labelled *C*, is dynamically distinct from the systemic redshift. Component *B* has an [N II]/Hα emission line ratio of 0.37 ± 0.05, which is indicative of star formation, although the presence of an underlying (2300 ± 250 km s^{-1}) Hα broad-line region suggests AGN activity or scattered light from an AGN. The velocity offset of the narrow line Hα from the systemic galaxy is $+50 \pm 50$ km s^{-1} and has a width of 360 ± 25 km s^{-1}, whilst the broad-line Hα is redshifted by $+800 \pm 150$ km s^{-1} (all linewidths have been deconvolved for the instrumental resolution).

Turning to the Lyα emission line map from the GMOS IFU observations (Fig. 1), we find an an extended, diffuse Lyα halo. Whilst the Lyα seems roughly to follow the I_{814}-band morphology, we also identify Lyα emission lying outside the optical extent of the galaxy (labelled *D* in Fig. 1). The spatial extent of the Lyα is $\sim$16 kpc, however, most interestingly the velocity of the emission line is placed $+270 \pm 40$ km s^{-1} redward of the systemic velocity of this system. We detect no significant velocity structure in the Lyα emission across the system (see Table 1).

Using a deep, 1.44-arcsec resolution 1.4-GHz map of the field from the VLA, Ivison et al. (2002) identified a compact radio source with a centroid that corresponds exactly to the location of component *B* in Fig. 1. This gives us confidence that this component is responsible for the far-infrared activity. The third component (labelled *C*) is offset from *A*/*B* by $+220 \pm 50$ km s^{-1} and has an upper limit of [N II]/H$\alpha \lesssim 0.05$ and a width of 320 ± 30 km s^{-1}. This indicates star formation rather than AGN activity, although there is also evidence for a broad-line Hα component at the same redshift as the broad line seen in component *B* (Fig. 2). This broad-line Hα may arise as part of the same scattered emission seen in the [O III] λ5007 emission in Smail et al. (2003). To attempt to identify which component hosts the AGN activity, we constructed a (wavelength-collapsed) white-light image from the datacube between 2.23 and 2.25 μm (i.e. the broad-line Hα emission) and compared this with the white-light image generated by collapsing the datacube between 2.215 and 2.225 μm (which includes the narrow-line Hα emission). Unfortunately, these two images look very similar and it is not possible to identify which component hosts the AGN.

The velocity offsets and spectral differences seen among the various morphological components immediately rules out the possibility that all are gravitationally lensed images of a single background source. Instead, it appears that N2 850.4 is a multi-component and complex merger. Assuming the velocity offsets arise owing to merging components in the potential well, we estimate a dynamical mass of $\gtrsim 2 \times 10^{11}$ M$_{\odot}$.

The velocity offsets from the Hα emission can be compared directly to the dynamics from the CO(4–3) and CO(7–6) observations of Neri et al. (2003) (see also Greve et al. 2005). It appears that the broad CO(4–3) emission arises from two components – a bright component at $z = 2.383$, and a fainter component at slightly higher redshift (at $z \sim 2.388$) which is located $\gtrsim$0.3 arcsec to the NE of the first component. Narrow CO(7–6) emission is also detected at the same position and redshift as the lower-redshift CO(4–3) emission. Assuming the CO(7–6) and the lower redshift CO(4–3) emission arise from warm, dense gas associated with *A* and/or *B* and the higher redshift CO(4–3) emission arises from component *C*, the velocity and spatial offsets are in excellent agreement with our IFU observations. Furthermore, this suggests that *A*/*B* and *C* all host gas reservoirs, with *B* being the most massive. The implied molecular gas mass from the CO observations is $\sim 5.5 \times 10^{10}$ M$_{\odot}$, thus the dynamical mass ($\sim 2 \times 10^{10}$ M$_{\odot}$) for N2 850.4 is approximately four times greater than the gas mass estimate, suggesting that this system has a high baryonic fraction in the central regions.

Using the Hα emission line as a star-formation rate indicator we can calculate the star-formation rate in each of the three components. For solar abundances and adopting a Salpeter IMF, the conversion between Hα flux and star-formation rate is SFR (M$_{\odot}$ yr^{-1}) = 7.9×10^{-35} L(Hα) W m^{-2} (Kennicutt 1998). This calibration assumes that all of the ionizing photons are reprocessed into nebular lines (i.e. they are neither absorbed by dust before they can ionize the gas, nor do they escape the galaxy). Using the narrow-line Hα emission line fluxes with this calibration we find that the star-formation rates of components *A*, *B* and *C* (uncorrected for reddening) are $\lesssim$30, 150 ± 30 and 140 ± 30 M$_{\odot}$ yr^{-1}, respectively. The total star-formation rate is a factor of $\gtrsim$10 less than the star-formation rate implied from the far-infrared luminosity, and implies approximately three magnitudes of dust extinction (e.g. Smail et al. 2004).

4 DISCUSSION AND CONCLUSIONS

The colours and morphology of N2 850.4 from our *HST* ACS and NICMOS imaging resemble that of a strongly lensed galaxy, however the lens interpretation is quickly ruled out from the Hα emission

maps which show that this system is made up of at least three dynamically distinct components separated by ∼1 arcsec (8 kpc) in projection and up to 220 ± 50 km s^{-1} in velocity. The ground- and space-based imaging data also shows a diffuse and asymmetric halo of material surrounding the galaxy. The Hα redshift of components A/B in Fig. 1 are in excellent agreement with previous CO and rest-frame UV long-slit observations which have measured the systemic redshift to be 2.384 (Neri et al. 2003; Smail et al. 2003; Greve et al. 2005). The presence of an underlying broad (∼2000 km s^{-1}) emission line (offset by ∼+800 km s^{-1}) in components *B* and *C* suggests AGN activity. Comparable narrow-line to broad-line velocity offsets are frequently seen in local Seyfert nuclei (e.g. Osterbrock & Shuder 1982; Corbin & Boroson 1996; Storchi-Bergmann et al. 2003) as well as high-redshift radio galaxies (e.g. Simpson, Rawlings & Lacy 1999). The third component detected in narrow-line Hα emission *C* is redshifted from the systemic by 220 ± 50 km s^{-1}. Combined with the high-resolution imaging, the complex morphology and dynamics of this system suggest a massive merger event that has presumably triggered a strong, obscured starburst and AGN activity.

The GMOS IFU observations show that N2 850.4 has an extended halo of Lyα emission. The Lyα halo has a spatial extent of ∼16 kpc and is redshifted relative to the systemic velocity by +270 ± 40 km s^{-1}. It is interesting to compare the Lyα emission from N2 850.4 with the giant sub-mm detected Lyα haloes LAB1 and LAB2 in the SSA22 field (Steidel et al. 2000; Chapman et al. 2001, 2004; Bower et al. 2004; Wilman et al. 2005). From our observations, N2 850.4 has a slightly lower integrated Lyα luminosity ($\gtrsim 3 \times 10^{43}$ erg s^{-1}) compared to LAB1 and LAB2 (1×10^{44} erg s^{-1} and 9×10^{43} erg s^{-1}, respectively), but is much more compact (LAB1 and LAB2 have areas of over 100 arcsec^2, i.e. 5000 kpc^2), however the limiting surface brightness of the GMOS observations are $\sim 5 \times 10^{-16}$ erg s^{-1} cm^{-2} arcsec^{-2} (significantly less than the surface brightness limit of LAB1 and LAB2 narrow-band imaging observations), and it is therefore possible that N2 850.4 is surrounded by a large-scale diffuse emission halo below the sensitivity limit of the GMOS IFU observations. Nevertheless, the Lyα emission from N2 850.4 is much more peaked than LAB1 and therefore this halo may represent a different evolutionary phase. Unfortunately, owing to the very different surface brightnesses of the systems and the large pixel scale of the SAURON IFU (which has 1.0 arcsec fibres), it is very difficult to compare the dynamics of the two systems directly (Bower et al. 2004). In terms of the wider environment, it is interesting to note that a second sub-mm detected galaxy has recently been detected in the same structure as N2 850.4 (at a distance of 2.5 Mpc; Chapman et al. 2005).

The observed velocity offset between Hα and Lyα emission is comparable to those seen in the spectra of rest-frame UV selected galaxies at $z \gtrsim 2$ (e.g. Teplitz et al. 2000; Pettini et al. 2001; Shapley et al. 2003) where they have been attributed to galactic-scale outflows produced by the collective effects of heating and outflows from supernovae. In this scenario, the Lyα appears redshifted owing to resonant scattering of photons from the inner surface of a receding shell of material. Such flows have been termed 'superwinds' by analogy with the wind seen in the spectra of local ultra-luminous infrared galaxies and local starburst galaxies (e.g. Keel et al. 2005; Martin 2005). If such winds can escape from the potential well, they can carry metals to large distances from the galaxy and deposit large amounts of energy in the intergalactic medium. These winds thus have important consequences for the metal enrichment of the Universe (Aguirre et al. 2001) and galaxy formation models (Benson et al. 2003). The key issue, however, is whether the wind material is localized within individual H II regions (in which case it may not escape the galaxy potential), or whether the expelled shell already envelops the complete galaxy. The latter interpretation is supported by Adelberger et al.'s (2003) observation of a small-scale anti-correlation between galaxies and Lyα absorption in QSO spectra (although, as those authors quote, the statistical significance of this result is modest). If it can be demonstrated that the superwind shell had already escaped from the galaxy disc, then it may have enough energy to escape the gravitational potential and distribute its energy metals widely across the Universe.

To distinguish between these scenarios, we must examine the spatial variation of the velocity offset between Hα and Lyα. Our data show no correlation between the emission wavelength of Lyα and the velocity variations clearly seen in Hα. This argues that the Lyα emission originates outside the individual components. If we were seeing the inner surface of a shell located well outside the galaxy we would expect a negligible velocity shear, and indeed our observations place a limit on the shear of $\lesssim$100 km s^{-1}.

We can also investigate how closely the morphology of the Lyα emission traces the star-forming regions of the galaxy. While the Lyα intensity map generally traces the I_{814}-band morphology, the diffuse extension labelled *D* in Fig. 1, has no counterpart in the I_{814}-band image. This component may be a dense knot in an outflowing shell and would be compatible with a model in which scattered Lyα photons are observed from the outflowing shell.

The data presented here support the idea that we are seeing wind material that has already escaped from the galaxy. It is interesting to compare the velocity offset in Lyα with the escape velocity of the galaxy. Using the dynamical mass estimate ($\sim 2 \times 10^{11}$ M$_\odot$) enclosed in a radius of ∼8 kpc we estimate the escape velocity to be $\gtrsim$500 km s^{-1} (assuming a central concentration of $c = 7$ for $z = 2.4$) (Navarro et al. 1997). Whilst this escape velocity exceeds that of the outflowing material, the fate of the outflow will depend on its present location (or, equivalently, its initial velocity). For example, if the outflow originated in the galaxy with an initial speed of ∼270 km s^{-1}, then it will surely rain back down on the galaxy. However, if, as we have argued, the shell is currently located outside the galaxy (i.e. $\gtrsim$10 kpc), then the escape velocity will be a factor of ∼2 less, in which case the outflow will probably escape the gravitational potential and distribute the gas much more widely in the environment. We also note that the UV-bright starburst in N2 850.4 is still relatively young (∼10 Myr; Smail et al. 2003) and therefore this material may still be accelerating into the inter-galactic medium. Future observations of a larger sample of these galaxies (at various evolutionary stages) may yield further information about the origin of the outflows and the size of the regions which they affect around them (Geach et al., in preparation).

Our observations suggest that the vigorous activity in N2 850.4 is arising due to an interaction between at least two distinct components. One of these contains warm, dense molecular gas and hosts an AGN, while the second appears to be less massive, but still contains substantial amounts of cold gas. The resulting gravitational tides resulted in a starburst and (actively fuelled) AGN activity. This activity has produced a wind that may be driving enriched gas out into the inter-galactic medium. Whilst these observations are based on a single galaxy, our results clearly show the power of combining optical and near-infrared observations to probe the power sources, masses and feedback processes in high-redshift, far-infrared luminous selected galaxies. The next step is to generate a statistically useful sample to gauge the prevalence of outflows from these massive galaxies, which may explain the processes that shape the galaxy

luminosity function and explain why only 10 per cent of baryons cool to form stars.

ACKNOWLEDGMENTS

We are very greatful to the referee, Seb Oliver, for his constructive report which significantly improved the content and layout of this paper. We would like to thank Brad Cavanagh, Peter Draper and Stephen Todd for useful discussions and help regarding the UIST IFU data reduction pipeline and Watson Varicatt and Sandy Leggett for observing the target with UIST IFU in UKIRT queue mode in 2003A. We would also like to thank Matt Mountain and Jean-Rene Roy for accepting the GMOS IFU programme for Science Demonstration, Inger Jørgensen and Kathy Roth for vital assistance in observing the target with GMOS, and Bryan Miller for useful discussion regarding the GMOS data reduction pipeline. We acknowledge Roger Davies and Gerry Gilmore, who were the joint PIs of the GMOS-DDT proposal. We also acknowledge useful discussions with Alastair Edge, Jim Geach, David Gilbank, Thomas Greve, Chris Simpson, Martin Ward and Richard Wilman. AMS acknowledges support from PPARC, IRS acknowledges support from the Royal Society, RGB acknowledges a PPARC Senior Fellowship and he Euro 3D Research Training Network. AWB acknowledges support from NSF AST-0205937 and the Alfred Sloan Foundation.

The United Kingdom Infrared Telescope (UKIRT) is operated by the Joint Astronomy Centre on behalf on the UK Particle Physics and Astronomy Research Council. STScI is operated by the Association of Universities for Research in Astronomy, Inc., under NASA contract NAS5-26555. Support for the Space Telescope Science Institute (MAST) for non-*HST* data is provided by the NASA Office of Space Science via grant NAG5-7584 and by other grants and contracts. The Infrared Telescope Facility (IRTF) is operated by the University of Hawaii under Cooperative Agreement no. NCC 5-538 with the National Aeronautics and Space Administration, Office of Space Science, Planetary Astronomy Program.

REFERENCES

Adelberger K. L., Steidel C. C., Shapley A. E., Pettini M., 2003, ApJ, 584, 45
Aguirre A., Hernquist L., Schaye J., Katz N., Weinberg D. H., Gardner J., 2001, ApJ, 561, 521
Alexander D. M. et al., 2003, AJ, 125, 383
Alexander D. M., Smail I., Bauer F. E., Chapman S. C., Blain A. W., Brandt W. N., Ivison R. J., 2005, Nat, in press
Allington-Smith J. R. et al., 2002, PASP, 114, 79
Balogh M. L., Pearce F. R., Bower R. G., Kay S. T., 2001, MNRAS, 326, 1228
Barger A. J., Cowie L. L., Smail I., Ivison R. J., Blain A. W., Kneib J.-P., 1999, ApJ, 117, 2656
Benson A. J., Bower R. G., Frenk C. S., Lacey C. G., Baugh C. M., Cole S., ApJ, 2003, 599, 38
Bower R. G. et al., 2004, MNRAS, 351, 63
Cavanagh B., Hirst P., Jenness T., Economou F., Currie M. J., Todd S., Ryder S. D., 2003, in Payne H. E., Jedrzejewski R. I., Hook R. N., eds, Astronomical Data Analysis Software and Systems XII. ASP Conf. Ser., Vol. 295, p. 237
Cen R., Ostriker J. P., 1999, ApJ, 514, 1
Chapman S. C., Smail I., Ivison R. J., Blain, 2001, ApJ, 548, L17
Chapman S. C., Smail I., Ivison R. J., Blain, 2002, MNRAS, 335, L17
Chapman S. C., Blain A. W., Ivison R. J., Smail I., 2003, Nat, 422, 695
Chapman S. C., Scott D., Windhorst R. A., Frayer D., Borys C., Lewis G. F., Ivison R. J., 2004, ApJ, 606, 85
Chapman S. C., Smail I., Windhorst R., Muxlow T., Ivison R. J., 2004, ApJ, 611, 732
Chapman S. C., Blain A. W., Smail I., Ivison R. J., 2005, ApJ, in press
Corbin M. R., Boroson T. A., 1996, ApJS, 107, 69
Dannerbauer H., Lehnert M. D., Lutz D., Tacconi L., Bertoldi F., Carilli C., Genzel R., Menten K. M., 2004, ApJ, 606, 664
Garnett M. A., Shields G. A., Skillman E. D., Sagan S. P., Dufour R. J., 1997, ApJ, 489, 63
Genzel R., Baker A. J., Tacconi L. J., Lutz D., Cox, P., Guilloteau S., Omont A., 2003, ApJ, 584, 633
Greve T. R., Ivison R. J., Bertoldi F., Stevens J. A., Dunlop J. S., Lutz D., Carilli C. L., 2004, MNRAS, 354, 779
Greve T. R. et al., 2005, MNRAS, in press (doi:10.1111/J.1365-2966.2005.08979.x)
Ivison R. J. et al., 2002, MNRAS, 337, 1
Keel W., Irby B., May A., Miley G., Golombek D., de Grijp M., Gallimore J., ApJS, in press
Kennicutt R. C., 1998, ARA&A, 36, 189
Koekemoer A. M., Fruchter A. S., Hook R. N., Hack W., 2002, in Arribas S., Koekemoer A., Whitmore B., eds, Proc. The 2002 HST Calibration Workshop. Baltimore, MD
Knudsen K., 2004, PhD thesis, Univ. Leiden
Martin C., 2005, ApJ, 621, 227
Navarro Julio F., Frenk C. S., White S. D. M., 1997, ApJ, 490, 493
Neri R. et al., 2003, ApJ, 597, L113
Osterbrock D. E., Shuder J. M., 1982, ApJS, 49, 149
Pettini M., Shapley A. E., Steidel C. C., Cuby J., Dickinson M., Moorwood A. F. M., Adelberger K. L., Giavalisco M., 2001, ApJ, 554, 981
Pope A., Borys C., Scott D., Conselice C., Dickinson M., Mobasher B., 2005, MNRAS, 358, 149
Ramsay-Howat S. et al., 2004, in Moorwood A. F. M., Iye M., eds, Proc. SPIE Vol. 5492, Ground-based Instrumentation for Astronomy. SPIE, Bellingham, p. 1160
Scott S. E. et al., 2002, MNRAS, 331, 817
Shapley A. E., Steidel C. C., Pettini M., Adelberger K. L., 2003, ApJ, 588, 65
Shure M. et al., 1993, AAS, 183, 11701
Simpson C., Rawlings S., Lacy M., 1999, MNRAS, 306, 828
Smail I., Ivison R. J., Blain A. W., 1997, ApJ, 490, L5
Smail I., Ivison R. J., Blain A. W., Kneib J. P., 2002, MNRAS, 331, 495
Smail I., Chapman S. C., Ivison R. J., Blain A. W., Takata T., Heckman T. M., Dunlop J. S., Sekiguchi K., 2003, MNRAS, 342, 1185
Smail I., Chapman S. C., Ivison R. J., Blain A. W., 2004, ApJ, 616, 71
Steidel C. C., Adelberger K. L., Shapley A. E., Pettini M., Dickinson M., Giavalisco M., 2000, ApJ, 532, 170
Storchi-Bergmann T. et al., 2003, ApJ, 598, 956
Swinbank A. M., Smail I., Chapman S. C., Ivison R. J., Blain A. W., Keel W., 2004, ApJ, 617, 67
Tecza M. et al., 2004, ApJ, 605, L109
Teplitz H. I. et al., 2000, ApJ, 533, 65
Webb T. M. A., Lilly S. J., Clements D. L., Eales S., Yun M., Brodwin M., Dunne L., Gear W. K., 2003, ApJ, 597, 680
White S. D. M., Rees M. J., 1978, MNRAS, 183, 341
Wilman R. et al., 2005, Nat, submitted

This paper has been typeset from a TEX/LATEX file prepared by the author.